Published in final edited form as:
J Mol Biol. 2009 May 22; 388(5): 954–967. doi:10.1016/j.jmb.2009.03.044.

Existence of a non-canonical state of iron-bound transferrin at endosomal pH revealed by hydrogen exchange and mass spectrometry

Cedric E. Bobst, **Mingxuan Zhang**[1], and **Igor A. Kaltashov**✉
Department of Chemistry, University of Massachusetts, Amherst, MA 01003

Summary

Transferrin is an enigmatic metalloprotein, which exhibits a profound conformational change upon binding of ferric ion and a synergistic anion (oxalate or carbonate). While the apo- and holo-forms of the protein have well-defined and stable conformations termed “open” and “closed,” certain aspects of transferrin behavior imply the existence of alternative protein states. In this work hydrogen/deuterium exchange was used in combination with mass spectrometry to map solvent-accessible surfaces of the iron-bound and iron-free forms of the N-lobe of human serum transferrin at both neutral and endosomal pH. While the deuterium uptake is significantly decelerated in the iron-bound state of the protein (compared to the apo-form) at neutral pH, the changes are distributed very unevenly across the protein sequence. Protein segments exhibiting most noticeable gain in protection map onto the inter-domain cleft region housing the iron-binding site. At the same time, protection levels of segments located in the bulk of the protein are largely unaffected by the presence of the metal. These observations are fully consistent with the notion of a metal-induced switch from the open to the closed conformation with solvent-inaccessible inter-domain cleft. However, differences in the exchange behavior between the apo- and holo-forms of transferrin become much less noticeable at endosomal pH, including the segments located in the inter-domain cleft region. Intriguingly, a significant patch in the cleft region becomes slightly less protected in the presence of the metal, suggesting that the holo-protein exists in the open conformation under these slightly acidic conditions. The existence of a non-canonical state of holo-transferrin was postulated several years ago; however, this work provides for the first time conclusive evidence that such alternative states are indeed populated in solution.

Keywords

Metal transport; transferrin; protein conformation; hydrogen/deuterium exchange; mass spectrometry

✉Address correspondence to: Igor A. Kaltashov, Department of Chemistry, University of Massachusetts-Amherst, 701 North Pleasant Street, Lederle Graduate Research Tower 701, Amherst, MA 01003, Tel (413) 545-1460, Fax (413) 545-4490, Kaltashov@chem.umass.edu.
[1]Present address: Schering-Plough Research Institute, 320 Bent Street, Cambridge, MA 02141

Introduction

Iron is one of a few metals whose availability is critical to all life forms due to its intimate involvement in key biochemical and physiological processes: most importantly, energy transfer and oxygen transport. Despite being one of the most abundant elements in the Earth's crust, iron's bioavailability is severely limited under aerobic conditions due to the extremely poor solubility of its oxidized form, ferric ion (Fe^{3+}). While a variety of strategies are employed by different organisms to facilitate iron uptake and retention, vertebrates rely on proteins from the transferrin family as a means to solubilize and capture iron in various biological fluids. Human serum transferrin (*h*Tf) is the only member of this family, which delivers its iron via receptor-mediated endocytosis.[1] In addition to iron, *h*Tf has the ability to bind a range of other metals with high affinity and also deliver them to tissues.[2] Since the *h*Tf receptor (TfR) is over-expressed on the surface of malignant cells due to their increased demand for iron, *h*Tf provides a major uptake route for several radiopharmaceuticals and imaging agents to tumors. Furthermore, the ability of *h*Tf to enter cells (*via* endocytosis) and especially to cross the blood-brain barrier (*via* transcytosis) has made it a focus of extensive efforts to achieve targeted delivery of other therapeutic agents into cancer cells via conjugation.[3; 4]

As most other transferrins, *h*Tf is composed of two highly homologous lobes, generally termed N- and C-lobe. Each lobe has a clamshell-like fold and contains a large cleft that binds Fe^{3+} and a synergistic anion (CO_3^{2-} or $C_2O_4^{2-}$). In each of the lobes the bound ferric ion is hexacoordinated, with four coordination sites provided by the protein (one glutamate, two tyrosines and one histidine) and the remaining two coordination sites provided by the synergistic anion. Crystal structures of several full-length transferrins and individual lobes reveal a significant conformational change upon iron binding, which results in a closing of the iron-binding cleft. These two distinct conformations of *h*Tf (commonly referred to as "open" and "closed") have different affinities for the receptor (TfR), with the closed conformation being the strong binder at neutral pH and, therefore, favoring association of iron-loaded *h*Tf with TfR at the cell surface.[5; 6]

Crystallographic data are particularly abundant for the N-lobe of *h*Tf (*h*Tf/2N), where a transition between the open and the closed forms of the protein involves a motion in the hinge region connecting two domains (NI and NII), bringing them into closer proximity and rotating one with respect to the other.[7; 8] While it is clear that such a transition is necessary to arrange the metal coordination site, mechanistic details of this process remain largely unknown.

A general mechanism of metal binding to proteins from the transferrin family was proposed several years ago by Baker *et al.*, which invokes the notion of conformational hopping between the two alternative states (open and closed) in both apo- and holo-forms of the protein.[9] The metal-free protein spends most of its time in the canonical open state, but transiently samples the closed conformation as well. According to this model, the metal ion initially binds the protein in the open conformation, but the next visitation to the closed state would effectively lock the system in the latter conformation, as it offers a more favorable metal coordination. A possibility of iron binding to the open conformation of transferrin was elegantly confirmed by Mizutani *et al.*,[10] who doped the crystal of apo-ovotransferrin N-lobe with a solution of iron complexed to NTA. The subsequent X-ray crystallographic analysis suggested that the protein retained the open conformation and only one domain (NII) participated in the iron binding. NTA anions and water molecules provided ligands to complete the hexacoordination sphere and compensate for the inability of side chains located on the NI domain to participate in metal binding.

Establishing the existence of these non-canonical states in solution proved to be a difficult task, since conventional experimental techniques provide limited information on conformational

dynamics of transferrin. Application of high-resolution NMR spectroscopy to obtain dynamic data on transferrin molecules is limited by the relatively large size of these proteins (35-80 kDa) and the presence of paramagnetic ferric ions. Dynamic processes associated with metal dissociation from transferrin molecules can be monitored using optical spectroscopic techniques, such as fluorescence;[11] however, these studies usually provide very limited structural information. Detailed structural information can be deduced from X-ray crystallographic data; however, this method is hardly suitable for characterization, or indeed detection of transient metastable species.

Electrospray ionization mass spectrometry (ESI MS) emerged recently as a powerful tool to probe structure and behavior of metalloproteins at a variety of levels.[12]. We utilized ESI MS in the past to monitor the composition of protein-metal complexes at neutral and endosomal pH, and thereby provide circumstantial evidence that the non-canonical states of transferrin may exist as metastable species in solution for extended periods of time.[13; 14] The behavior of the protein-metal complexes detected at endosomal pH in the absence of metal chelators was consistent with the notion that a non-canonical state (open conformation for the holo-form of *h*Tf/2N) was present in solution; however, no structural data could be obtained at the time to prove that hypothesis. In the present work we use hydrogen/deuterium exchange (HDX) as a tool to probe changes of the solvent accessibility of various segments of *h*Tf/2N following metal removal at both neutral and endosomal pH. This study provides conclusive evidence for the existence of iron-bound *h*Tf/2N that adopts an open conformation in solution. In addition to its obvious role in metal binding and release, the existence of non-canonical states of transferrin could also be an important factor modulating the interaction of this protein with its receptor throughout the various stages of endocytosis.

Results

HDX MS of hTf/2N at neutral pH

Our earlier measurements of global HDX kinetics of the apo- and holo-forms of *h*Tf/2N at pH 7.4 revealed a significantly higher rate of deuterium uptake by *h*Tf/2N in the absence of ferric ion. The lower overall backbone protection of the apo-form of *h*Tf/2N is in agreement with the structural (crystallographic) data at neutral pH, which reveal a more solvent-accessible conformation of the protein in the absence of iron.[7] In order to prove that the difference in global exchange rates between the two forms of *h*Tf/2N arises from the difference in their conformations, local HDX MS measurements (at the peptide level) were carried out in this work. Such measurements can be implemented by fragmenting the protein either in solution under slow exchange conditions using acidic proteases[15] or in the gas phase using various methods of ion dissociation.[16; 17] While collisional activation of *h*Tf/2N ions in the gas phase generates abundant fragment ions, the sequence coverage is very uneven due to the presence of multiple disulfide bonds.[18] Therefore, local measurements of deuterium incorporation were carried out in this work using proteolysis (either pepsin alone or pepsin in combination with fungal protease type XIII[19]) and chemical reduction of disulfide bonds under slow exchange conditions (see ***Materials and Methods*** for more detail).

Overall, 130 peptide fragments were detected, ranging in size from 0.3 to 6.7 kDa, and 41 of the most abundant with maximal sequence coverage were used to characterize local exchange in *h*Tf/2N at neutral pH. The overall sequence coverage was high despite the apparent difficulty in complete reduction of all of the eight disulfide bonds present in *h*Tf/2N. Sequence coverage was 76% for both apo and holo samples and included most of the residues playing an important role in metal binding: notably all four residues directly involved in coordinating iron (D63, Y95, Y188, H249), one of the two residues that bind the synergistic anion (R124), and both lysine residues forming the di-lysine trigger (K206, K296).[20] The majority of the missing sequence is located in the NII domain.

Figure 1A shows the raw mass spectral data obtained for four peptides demonstrating markedly different patterns of deuterium uptake revealed by the increase in their masses as a function of exchange time in solution. The differences are more readily compared after calculating the average mass for the peptides at each time-point and producing kinetic plots of mass increase vs. exchange time (Figure 1B). Since the total number of exchangeable amides is known, the kinetic data can also be represented on the y-axis as a fraction of the theoretical maximum exchange level.

A difference in exchange is clearly observed between the two forms of the protein (apo- and holo-) for three out of the four peptides shown in Figure 1, which correspond to segments [205-211] (labeled *i* in Figure 1), [61-67] (*iii*), and [183-191] (*iv*). In each of these cases, the apo-protein displays lower protection (thereby a greater increase in mass) than its holo counterpart, suggesting their importance in iron binding. Indeed, this is confirmed when we map the peptides to the available crystal structure, which shows peptides *i*,*ii*, and *iv* map to different regions along the binding cleft (Figure 1C). This behavior contrasts with that of peptic fragment [215-225] derived from the external loop of *h*Tf/2N (*ii* in Figure 1), a region not involved in iron binding. Deuterium uptake by this peptide clearly is insensitive to the presence of the ferric ion.

In order to visualize the distribution of protected amide hydrogen atoms across the protein sequence and to simplify the data presentation, a single representative time point (5 min) was chosen from the HDX MS dataset acquired at neutral pH. The location of the 41 analyzed peptides are illustrated by horizontal bars below the corresponding primary structure of *h*Tf/2N and were colored based on their extent of deuterium incorporation (protection) after 5 minutes for the apo sample (Figure 2). Results from the individual fragments were consolidated into a single line by placing smaller overlapping peptides on top of the larger peptides.

The diagram presented in Figure 2 clearly shows that the backbone flexibility of *h*Tf/2N is distributed very unevenly across the protein amino acid sequence. There are five notable regions, in which the extent of deuterium incorporation is very low following 5 min of exchange (and fails to reach a 40% level even after 2 hours of exchange, data not shown) in both apo- and holo-forms of *h*Tf/2N. Comprised primarily of residues 190 – 211 and 226 – 253 as well as three smaller segments (72 – 84, 123 – 127, 320 – 323), these slow exchanging segments represent a less dynamic (protected) core of *h*Tf/2N, and include various β-sheets and helices within both the NII and NI domains. This protected core contains only one (of four) residue that directly participates in binding ferric ion (H249), and also includes a residue critically important for metal binding, R124, which forms a salt bridge to the synergistic anion in the crystal structure of *h*Tf/2N. Peptic fragments containing K206, the presumed low pK_a element of the di-lysine trigger, also belong to the protected core, although they show a dramatic increase in protection upon metal binding. Peptic fragments containing the other element of the di-lysine trigger (K296) do not appear to be affected by the metal binding.

Overall the local exchange patterns are consistent with earlier global HDX MS studies, as a significant number of peptides display less protection in the apo-form of the protein. The spatial resolution gained through the local experiments can readily be observed by mapping the HDX MS data (5 min exchange) onto available crystal structures of *h*Tf/2N (Figure 3). Both open and closed conformations were used to produce maps to help visualize distribution of backbone flexibility in the regions of the protein that would not be seen otherwise in the “canonical” conformation (*e.g.*, cleft region in the holo-form of *h*Tf/2N). This mapping produces three-dimensional patterns consistent with a more solvent accessible open conformation for the apo-protein, as more protection was afforded to the metal binding cleft in the presence of iron. In addition to the anticipated deceleration of the deuterium uptake within the metal binding cleft, several other segments of *h*Tf/2N display increased protection in the holo-form, most

noticeably in the NII domain. Intriguingly, two short segments in the NI domain (43-46 and 68-72) deviate from this trend by displaying drastically less protection in the holo-form of *h*Tf/2N.

HDX MS of hTf/2N at endosomal pH

The *in vivo* metal release from transferrin occurs within minutes in the mildly acidic environment (pH 5.5) of endosomes;[21] however, iron remains bound to *h*Tf/2N for hours at endosomal pH in the absence of chelators and non-synergistic anions.[13] The extremely slow metal dissociation from *h*Tf/2N under these conditions allows the conformational dynamics of the iron-bound form of the protein to be characterized by HDX MS and compared to the apo-state. Two alternative methods were employed for comparison of global exchange, continuous on-line HDX MS measurements and HDX followed by quench and MS measurements under the slow exchange conditions. The former technique allows the back-exchange to be completely avoided, while the latter offers the advantage of higher quality of MS measurements, since the protein denaturation under the slow exchange conditions leads to a more abundant ionic signal (and, consequently, higher signal-to-noise ratio) in ESI MS. The global exchange data acquired by both methods reveal remarkably similar kinetic profiles of deuterium uptake by both forms of *h*Tf/2N (Figure 4), in a stark contrast to their behavior at neutral pH (*vide supra*).

The magnitude of deuterium incorporation measured in the continuous infusion HDX MS experiments is significantly higher, as both backbone amide hydrogen atoms and labile hydrogen atoms of side chains contribute to the pool of exchangeable hydrogen atoms. The side chain contribution is lost when HDX is followed by quench and MS measurements under the slow exchange conditions, since the exchange of most labile hydrogen atoms on side chains remains relatively fast under the "quench" conditions.[22] Once the side chain correction is made, the two methods yield very similar plots of exchange kinetics of the backbone amide hydrogen atoms of *h*Tf/2N at pH 5.5 (Figure 4Importantly, the exchange incongruence observed for the two forms of the protein (apo and holo) at neutral pH 7.4 is all but eliminated at the endosomal pH.

The insensitivity of the global HDX kinetics to the iron status of *h*Tf/2N is consistent with the notion of structural similarity between the apo- and holo-protein at the endosomal pH. However, the definitive evidence of the existence of the putative "open" state of iron-bound *h*Tf/2N can only be provided by comparing the local patterns of deuterium incorporation in the iron-bound and iron-free forms of the protein. Barring very few exceptions, kinetics of deuterium uptake at the local level does not reveal noticeable difference between the apo- and holo-forms of *h*Tf/2N. One of the exceptions is shown in Figure 1B, where a protein segment [61-67] appears to be more protected in the presence of iron following short periods of exposure to the exchange buffer, although this additional protection is eliminated following 10 min of exchange. This is in sharp contrast to the protein behavior at neutral pH, where the presence of iron exerts a significant influence on exchange patterns of a large number of protein segments over extended timescale.

A more detailed comparison of the local backbone protection patterns of apo- and holo-*h*Tf/2N at pH 5.5 is presented in Figure 5, where all observed peptic fragments are mapped to the tertiary structure of the two canonical forms of *h*Tf/2N and colored according to the extent of deuteration following 5 min of exchange. These peptides, also viewable as mapped to the protein sequence (Supplemental Figure S1), reveal a very high degree of similarity between the protection patterns of the iron-free and iron-bound forms of the protein. In order to enable a meaningful comparison of the two endosomal forms of *h*Tf/2N to those at neutral pH (shown in Figures 2 and 3), a set of pH 5.5 data at a longer exchange time (180 min) was chosen to offset the difference in the pH-dependent intrinsic (chemical) exchange rates for backbone

amides.[23] We utilized an additional protease (fungal protease XIII) to collect data at pH 5.5 in attempt to improve upon sequence coverage observed for pepsin alone at pH 7.4. Although the peptide map of *h*Tf/2N obtained in these experiments (Supplemental Figure S1) is not identical to the peptic map generated in the course of HDX studies at neutral pH, there is a very significant similarity both in terms of the fraction of the protein sequence covered (75%) and the specific polypeptide segments represented by the 38 peptic/fungal protease XIII fragments. Moreover, our analysis relies on the direct comparison of apo and holo data at each pH separately; therefore the observed difference in peptides produced does not limit the quality of our analysis. The extent of deuterium uptake displayed by several peptide fragments following 180 min exchange at pH 5.5 is comparable to that following a 5 min exchange at pH 7.4 (*e.g.*, peptic fragment [215-225] in Figure 1). Nevertheless, the protection was noticeably lower for the majority of observed peptide fragments at endosomal pH (following the adjustment of the exchange time scale to offset the difference in the intrinsic exchange rates), most likely reflecting an increase of the backbone flexibility under the mildly acidic conditions.

Proteolytic fragments whose deuterium content was analyzed following 180 min exchange at endosomal pH were color-coded (according to the displayed level of deuterium uptake) and mapped onto the amino acid sequence of the protein (Supplemental Figure S2) and the two canonical conformations of *h*Tf/2N (Supplemental Figure S3). These maps reveal a remarkable degree of similarity between the deuterium incorporation patterns of the apo- and holo-forms of *h*Tf/2N. While consistent with the HDX MS data obtained at the shorter exchange time at endosomal pH, this observation is a dramatic departure from the protein's behavior at neutral pH. Indeed, only four regions of *h*Tf/2N can be seen where the protection is affected by the presence of iron. The only difference that is observed at pH 5.5 in the cleft region (where the contrast between the apo- and holo-forms was most striking at neutral pH, *vide supra*) corresponds to a short segment incorporating one of the elements of the di-lysine trigger (K296). Interestingly, presence of iron makes this segment less protected. A few other segments (all located outside of the metal binding cleft region) also exhibit a slight acceleration of deuterium uptake in the presence of iron.

Discussion

Backbone protection at neutral pH and its relation to iron binding

Metal-induced conformational transitions in transferrin became a paradigm of large-scale changes of protein higher order structure induced by small ligands. In all studied proteins from this family the iron-bound state is represented by a "closed" conformation where a movement in the hinge region connecting two domains brings them into close proximity, thereby closing the inter-domain cleft and arranging the requisite geometry of the iron-binding site. This is contrasted to the "open" conformation characteristic of the metal-free states, where no interface exists between the two domains, making it impossible for the metal ion to achieve "proper" coordination by recruiting the side chains residing on two distant domains (*e.g.*, D63 and Y95 in NI and Y188 and H249 in NII domains of *h*Tf/2N). A transition from the closed to the open conformation of *h*Tf/2N at endosomal pH is induced by the dilysine trigger (K206-K296), where protonation of both side chains is expected to give rise to a very significant enthalpic penalty for the closed state of *h*Tf/2N.[20] A somewhat similar pH-sensitive element was also found in the C-lobe of *h*Tf, although it consists of three, rather than two, amino acid residues.[24] In this latter case protonation of the two basic residues of the triad at endosomal pH is viewed as a major enthalpic factor driving a transition from the closed form of the lobe to the open one to minimize electrostatic repulsion.

Iron release from the protein at endosomal pH had been traditionally viewed as a consequence of these conformational transitions, which necessarily destroy the metal ion coordination spheres. However, iron remains bound to *h*Tf/2N with a half-life greater than 3 hours at

endosomal pH in the absence of chelating agents.[13; 25] Addition of a chelating agent leads to a facile removal of iron from the protein, a fact that prompted a suggestion that ferric ion may remain bound to the protein even after activation of the pH-sensitive element triggers its transition to the open conformation.[13] In this case the inevitable disruption of the coordination sphere leading to the metal's inability to interact with all four iron-coordinating side chains (D63, Y95, Y188 and H249 in *h*Tf/2N) may be partially offset *via* recruitment of ubiquitous anions (*e.g.*, acetate) as surrogate ligands.

While the stability of an iron-bound open conformation of transferrin in the solid state was demonstrated by Mizutani *et al.*,[10] there was no solid evidence that such non-canonical states do exist in solution. Hydrogen-deuterium exchange is a powerful tool that allows presence of various conformations to be detected in solution, especially under conditions favoring correlated exchange.[26; 27] However, even uncorrelated exchange provides an opportunity to characterize protein conformations and observe transitions among them. Spatial distribution of the backbone protection in the holo-form of *h*Tf/2N (Figure 3A, C) identifies an internal patch in the inter-domain region surrounding the iron-binding site as the least dynamic segment of the protein. Iron binding to *h*Tf/2N clearly exerts a profound influence on the backbone protection in this region of the protein, as this segment displays the most significant difference when the apo- and holo-forms of the protein are compared to each other (Figure 3E, F). While this observation is not particularly surprising (the open conformation of *h*Tf/2N is indeed expected to favor faster exchange in the inter-domain cleft, especially in the protein segments surrounding the iron-binding site), it certainly lends credibility to the notion of HDX MS being capable of making a distinction between the two alternative conformations in solution.

Much less trivial conclusions are produced by analysis of the protein segment locations that exhibit lower-than-average stability in holo *h*Tf/2N. While two of such segments correspond to peripheral loops (*e.g.*, [Y84→Q92] and [R254→L262]) and are located far outside of the cleft region, the placement of two segments with highly labile backbone amides is rather curious. Specifically, a very short segment with anomalous flexibility [S44→L46] (colored red in Figure 3C) is positioned right at the edge of the inter-domain interface formed upon closing the cleft. In a three-dimensional structure of the closed form of *h*Tf/2N it is part of a small and well defined "low protection" patch at the edge of the NII domain. The other part of this patch is formed by the [Y68→L72] segment. A better view of this segment mapped to the closed conformation of *h*Tf/2N is shown in Figure 6A. It may seem counterintuitive that a protein segment involved so intimately in defining the fringe of the inter-domain interface in metal-bound state of *h*Tf/2N exhibits a higher-than-average rate of deuterium incorporation.

However strange this behavior may seem, local and limited increase in backbone flexibility may be an important factor enhancing the ability of *h*Tf/2N to bind and retain ferric ion via stabilization of the closed conformation of the protein. While structural disorder in general and increase in backbone flexibility in particular had been viewed traditionally as destabilizing factors, which affect negatively both folding and binding, a very different view begins to emerge from several recent studies.[28; 29] Indeed, protein flexibility plays a generally underestimated role in a range of binding processes,[30] which are generally characterized by unfavorable entropy changes opposing favorable enthalpic contributions. Therefore, decreased entropic cost of the association process necessarily translates into higher affinity.[31]

Although the conformational switch from the open to closed state of *h*Tf/2N triggered by iron binding lies outside of the paradigm of induced fit interaction as applied to the protein-receptor binding, many parallels between the two processes can be clearly seen. Indeed, closing the iron-binding cleft formed by two protein domains that do not interact in the open conformation leads to the formation of an interface akin to that encountered in promiscuous protein-protein associations. Formation of the latter is known to benefit from contributions of configurational

entropy.[32] Therefore, it seems plausible that limited local entropy release provides an important contribution to the free energy of the closed conformation of *h*Tf/2N.

Intriguingly, the flexible loop [S44→L46] is a part of a highly elaborate element of the tertiary structure of NII domain formed by two repeating strand/helix motifs (Figure 6A), which is placed right at the edge of the inter-domain interface as a result of cleft closure. In addition to the hydrogen bond network between the two β-strands (typical of parallel β-sheet), additional reinforcement of this element of tertiary structure comes from two disulfide bonds (C9-C48 and C19-C39) connecting each β-strand to a helix. Such reinforcements apparently make this structural element very stable, allowing it to survive the large-scale conformational transition (from the open to the closed state) with minimal perturbations of the core structure. This structural stability is evidenced by comparison of this region in the open and closed form of crystal structures (Figure 6B, C), where a calculated backbone RMS of residues 25→55 yields the small value of 0.48. However, a completely inflexible structure is likely to be detrimental to the protein's ability to form a stable interface between the two domains. Therefore, increased flexibility in the loop regions (especially those involved in interface formation) is likely to become a factor enhancing the interaction between the two domains via a favorable entropic contribution.

We note that the [S44→L46] loop is not the only protein segment that becomes more flexible following iron binding to *h*Tf/2N. Another segment exhibiting similar behavior (although to a somewhat lesser extent) is [Y68→L72]. Unlike [S44→L46], it does not form a loop, but is a C-terminal part of an α-helix formed by residues 63→72. Intriguingly, located at the opposite end of this helix is residue D63, whose side chain participates in coordinating ferric ion in the holo-form of *h*Tf/2N. The protein segment representing the immediate neighborhood of D63 (including the N-terminal part of helix 63→72) gains protection as a result of iron binding to the protein. It seems plausible that relaxation of the other end of this helix is a mechanism that provides additional entropic contribution to the metal binding and stabilization of the inter-domain interface. It is interesting to note that plasticity was theorized in this region to explain the ability of a D63E mutation to still bind iron.[33] Therefore it appears that the flexibility we identified in this region not only plays a role in stabilizing holo *h*Tf/2N, but also introduces, as a side effect, a degree of adaptability to the binding pocket. Intriguingly, a short segment [Y85→Q92] adjacent to another residue participating in iron coordination (Y95) also displays higher-than-average flexibility in the holo-form of *h*Tf/2N, while the immediate neighborhood of Y95 is highly protected (Figure 2). No significant differences between the apo- and holo-forms of *h*Tf/2N are seen at two other iron-binding sites (Y188 and H249).

In summary, a comparison of the local exchange patterns of the apo- and holo-forms of *h*Tf/2N at neutral pH provides clear evidence of two different conformations in solution. While the hydrogen exchange kinetics are accelerated in most protein segments following the removal of iron from *h*Tf/2N, the most striking difference is observed in the segment surrounding the iron binding site. The dramatic change in the rate of deuterium incorporation within this region is congruent with the expected decrease of backbone amide protection in the cleft region following the transition from the closed to the open conformation. At the same time, increased backbone flexibility within the few short segments of the protein located at the cleft edge is consistent with the notion of stabilizing the inter-domain interface in the iron-bound state of *h*Tf/2N by favorable entropic contributions at several key locations.

Backbone protection at endosomal pH is largely insensitive to iron binding

Unlike exchange at neutral pH, global kinetics of deuterium uptake by *h*Tf/2N at endosomal pH is insensitive to the presence of iron in the system (Figure 4), despite the protein's ability to retain iron under these conditions in the absence of metal chelators.[13; 14] A look at the spatial distribution of deuterium incorporation at endosomal pH also reveals a very minimal difference

between the apo- and holo-forms of *h*Tf/2N, in a sharp contrast to the local protection patterns observed at neutral pH (*vide supra*). Few segments can be found in the protein sequence where the levels of deuterium content following 5 min of exchange in solution are affected by the presence of iron (Supplemental Figure S1). Even in those segments the protection difference between the apo- and holo-forms of *h*Tf/2N is not very significant, exceeding 30% difference in only three amides (Y68→A70), which demonstrated a marked increase in exchange for holo *h*Tf/2N). In comparison, the difference in maximum deuteration levels at pH 7.4 exceeded 30% in 4 distinct regions composed of 19 amides as a result of iron introduction to the system. Most importantly, the extended patch in the cleft region that showed a dramatic increase of protection in the presence of iron at neutral pH does not show any detectable difference in the rate of deuterium uptake, strongly suggesting that the iron-bound form of *h*Tf/2N either fails to assume a closed conformation or else samples it only transiently.

Although the spatial distribution of backbone amide protection in both forms of *h*Tf/2N at endosomal pH (Supplemental Figure S2) is qualitatively very similar to that of the holo-form of the protein at neutral pH (Figure 2) following the same exchange time in solution, these two diagrams cannot be used to directly compare the stability of the protein backbone. Indeed, the amide exchange rate under near-native conditions almost always follows the so-called EX2 exchange regime, where the rate of exchange is controlled by both thermodynamics of the unfolding processes (exposing amide hydrogen atoms to the solvent) and the intrinsic exchange rate of the exposed amides:[34]

$$k_{HDX} \cong k_{int} \cdot \frac{k_{\text{opening}}}{k_{\text{closing}}} = k_{int} \cdot K_{\text{unfolding}},$$

with k_{int} displaying strong pH dependence.[23] Lowering the pH from 7.4 to 5.5 decreases the intrinsic exchange rate k_{int} by a factor of 60. Therefore, similar levels of deuterium incorporation indicate a 60-fold increase in $K_{\text{unfolding}}$ at endosomal conditions.

A meaningful comparison of HDX patterns observed at two different pH levels can only be made if the exposure time is adjusted to offset the difference in k_{int} values, so that any observed difference in k_{HDX} could be ascribed to changes in the unfolding equilibrium constant $K_{\text{unfolding}}$. In order to do this, local protection patterns recorded following 5 min of exchange at pH 7.4 (Figure 2) were compared to those obtained at pH 5.5 following 180 min of exchange (Supplemental Figure S3). The comparison of the protection maps clearly suggests that the holo-form of *h*Tf/2N is significantly less dynamic at neutral pH compared to both iron-bound and metal-free forms of the protein at endosomal pH. At the same time, there is significant qualitative similarity between the protection patterns of the apo-*h*Tf/2N at neutral pH and those of both forms of the protein at endosomal pH, although the former appears to be more protected overall. This observation is also consistent with the notion of both iron-bound and metal-free forms of *h*Tf/2N populating the open conformation at endosomal pH.

The existence of a non-canonical conformation of Fe^{3+}·*h*Tf/2N was postulated some time ago, based on the circumstantial evidence produced by direct monitoring of iron dissociation from this protein by ESI MS.[13] It was noticed that ferric ion remained bound to the protein for extended periods of time, as long as no chelating agents were present in solution. Addition of a physiological chelator (citrate) resulted in facile removal of iron from the protein at endosomal pH even when sub-physiological concentration levels of citrate were employed. Increase of the citrate concentration to physiological levels resulted in nearly complete removal of iron from *h*Tf/2N on the time scale of several minutes.[13] A suggestion was made that lowering the pH to endosomal levels does induce a transition from the closed to the open conformation, while failing to induce iron dissociation from the latter. In order for this to be

accomplished, a chelating agent must compete with the protein, whose association with iron in the open conformation is already compromised due to the inevitable replacement of two (out of four) metal-coordinating residues with weaker surrogate ligands (ubiquitous anions present in solution). This scenario is only possible in the open conformation of *h*Tf/2N, since ferric ion is sequestered from chelating agents in the inter-domain cleft in the closed state of the protein. However, direct evidence of the existence of the non-canonical iron-bound open conformation of transferrin in solution was lacking.

Previously, Mizutani *et al.* demonstrated that an open state of ovo-transferrin N-lobe can indeed be forced to bind ferric ion.[10] However, the mobility of the protein in this case was severely restricted, since it remained in a solid (although highly hydrated) state throughout the entire experiment (iron was introduced to the protein by soaking the apo-protein crystal with concentrated Fe^{3+}- NTA solution). Therefore, the failure of iron-bound protein to assume a canonical (closed) conformation observed by Mizutani *et al.* is likely to be attributable to the influence of packing forces in the crystal. Likewise, failure of human serum transferrin to adopt a canonical closed conformation upon binding UO_2^{2+} reported recently by Vidaud *et al.* is most likely caused by the steric constrains imposed on the protein by the uranyl cation due to its large physical dimensions.[35]

In the present work, the conformation of *h*Tf/2N was not externally constrained in any way, yet the iron-bound protein failed to adopt the canonical closed conformation at endosomal pH. Direct evidence to support the non-canonical state of human serum transferrin N-lobe in solution has very important and wide-ranging implications. First and foremost, it lends strong support to a conformational hopping model as a paradigm describing the large-scale conformational changes accompanying transferrin's interaction with its metal ion.[9] Indeed, transient sampling of the non-canonical conformations postulated in the conformational hopping model (*i.e.*, closed conformation by the apo-protein and open conformation by the holo-protein) provides a plausible mechanism of metal binding to and dissociation from transferrin. While these states are populated only transiently under physiological conditions, it was expected that certain conditions may increase their lifetime in solution, leading to metastable non-canonical states. The open conformation of Fe^{3+}·*h*Tf/2N is one of these non-canonical states, through which both metal binding (at neutral pH) and release (at endosomal pH) is likely to occur. The latter process is facilitated under physiological conditions by chelating agents, while their absence in solution gives rise to metastable Fe^{3+}·*h*Tf/2N existing in the open conformation, as demonstrated by the results of this study.

Second, the existence of the non-canonical states of transferrin has profound implications for the interaction mechanism of this protein with its receptor (TfR). TfR has the ability to discriminate between the apo- and holo-forms of Tf at the cell surface and in the endosome by binding strongly to iron-loaded protein at neutral pH, while displaying higher affinity to its iron-free form at endosomal pH.[36] Despite the obvious preference of TfR for the closed conformation of Tf at neutral pH,6; 37 a weaker interaction also exists between apo-Tf and TfR under these conditions, as suggested by earlier spectroscopic measurements5 and our own recent ESI MS studies (Leverence, *et al.*, manuscript in preparation). Likewise, while the endosomal pH favors recognition of the open conformation of Tf by TfR, a weaker association between diferric Tf and TfR is also observed. Given the conclusions of the present study, the latter observation is not all that surprising. Indeed, due to the structural similarity of the two Tf lobes and their common origin, it seems plausible that the iron-bound C-lobe can also populate the non-canonical open conformation at mildly acidic pH. Presence of such states of Fe_2Tf at endosomal pH will certainly provide a basis for Fe_2Tf/TfR recognition and binding.

Conceivably, analogous processes (population of non-canonical states by apo-Tf) may provide rationale for the observed (albeit weak) Tf/TfR interaction at neutral pH. At the same time, the

lack of such conformational flexibility may arrest Tf binding to its receptor under similar conditions.[35] Therefore, conformational promiscuity of transferrin observed in our study is likely to be an important factor modulating its interaction with the receptor, not limited to initial recognition, but in directing the entire process of iron delivery to cells via receptor-mediated endocytosis.

Materials and Methods

Sample Preparation

Stock solutions of apo and holo hTf/2N were buffer exchanged into 20 mM ammonium bicarbonate by repeated concentration and dilution using centrifugal membrane filters with a molecular weight cut off (MWCO) of 10K (Amicon, Millipore). The final concentration of the stock *h*Tf/2N was 20 $mg^{-1}ml$.

Instrumentation

All MS measurements were carried out with a hybrid quadrupole/time-of-flight mass spectrometer (QStar-XL, MDS Sciex/Applied Biosystems, Toronto, Canada) equipped with a standard Turbospray™ source.

Global HDX

Two alternative methods were employed for comparison, continuous online HDX MS measurements and HDX followed by quench and MS measurements under the slow exchange conditions. In both methods HDX was initiated by diluting the protein stock solution 20 fold into exchange buffer (50 mM ammonium acetate D_2O, pD 5.5 uncorrected for the isotope effect) at 25 °C. In the online method, deuterium incorporated within the protein was directly measured over a four minute window centered at the times indicated. In the quench method, HDX was first slowed by reducing the temperature in an ice bath for 30 seconds and then dropping the pH to 2.5 by adding four times the volume of an ice cold 0.15 % formic acid, 50 % methanol solution. MS measurements were then immediately recorded while keeping the syringe and tubing cold with ice packs. Data were processed using the software Bioanalyst (Applied Biosystems). Standard errors were calculated from triplicate measurements at a single representative time point for each method.

Peptide Resolved HDX Measurements

HDX was initiated by diluting the protein stock solutions 20-fold into exchange buffer (50 mM sodium phosphate D_2O, pD 7.4 or 5.5 uncorrected for the isotope effect) equilibrated to 25 ° C. At a designated time an aliquot of the solution was placed in an ice bath for 30 sec and then an equal volume of pre-chilled quench solution (3.6 M guanidine HCl, 0.5 % trifluoroacetic acid, 50 mM tris(2-carboxyethyl) phosphine HCl) was added and rapidly mixed, yielding pH 2.5. All subsequent steps were performed in an ice bath. The quenched sample was digested online using POROS (Applied Biosystems) immobilized protease prepared in house using a setup described elsewhere,38 with either pepsin alone (pH 7.4 data) or in combination with fungal protease type XIII19 (pH 5.5 data). The proteases were packed in stainless steel 50 × 2.1 mm columns as per the POROS-20AL recommended instructions. The digestion was performed at a flow rate of 0.16 ml min^{-1} using 0.1 % formic acid as the mobile phase. The resulting peptides were collected and desalted with an inline nanotrap cartridge then resolved by a C18 column (Armor Advance, 5 μm, 50 × 2.1 mm) using a rapid gradient from 5% to 65% acetonitrile containing 0.1 % formic acid and a flow rate of 0.3 ml min^{-1}. The total time for the digest and desalting was 3 min, all peptides had eluted from the C18 column by 9 min.

Peptide Resolved HDX Analysis

Proteolytic peptides were identified using a combination of exact mass and MS/MS data for unlabeled protein utilizing a shallower elution gradient. The extent of deuterium incorporation was calculated by monitoring the average mass increase for each identified peptide. The theoretical maximum deuterium incorporation value was calculated for each peptide based on the dilution factor and number of exchangeable amides, with the assumption that exchange of N-terminal amide is lost by back exchange during sample workup.[39] Peptide level data collected for pH 5.5 were generated using a combination of pepsin and fungal protease type XIII in tandem. This resulted in a different peptide map compared to the pepsin-only map generated for the pH 7.4 data, though 20 of the peptides analyzed were common under both digest conditions and the amount of sequence covered was similar at 76%. X-ray solved crystal structures for both apo[7] and holo[8] *h*Tf/2N were used to visualize the location of the peptides we observed. This experimental scheme allowed the standard error of peptide-level HDX MS measurements to be contained within 5% (estimate based on HDX MS data collected in triplicate to ensure the precision of mass measurements).

Leucine Enkephalin (LE), a pentapeptide with sequence YGGFL, was used as a model peptide to ensure that Fe^{3+} has no effect on the instrinsic H/D exchange rate under slow exchange conditions. At time 0, a 20 μM solution of LE in the absence or presence of 100 μM ferric chloride was diluted 20 fold into a deuterated solution emulating standard quench conditions (D_2O:acetonitrile:formic acid - 70:30:0.1; on ice). This was infused directly into the mass spectrometer and data was recorded for 15 minutes to monitor the resulting change in mass of LE. Plots of deuterium incorporation versus time for these experiments did not exhibit a statistically meaningful difference (Figure S4).

Supplementary Material

Refer to Web version on PubMed Central for supplementary material.

Acknowledgments

This work was supported by a grant from the National Institutes of Health R01 GM061666. The authors are very grateful to Dr. Anne B. Mason (Department of Biochemistry, University of Vermont Medical School, Burlington, VT) for many helpful discussions and providing *h*Tf/2N samples.

Abbreviations Used

Tf	transferrin
*h*Tf	human serum transferrin
*h*Tf/2N	recombinant N-terminal lobe of human serum transferrin
TfR	transferrin receptor
MS	mass spectrometry
ESI	Electrospray ionization
HDX	hydrogen/deuterium exchange
NTA	nickel-nitrilotriacetic acid

References

1. Aisen P. Transferrin, the transferrin receptor, and the uptake of iron by cells. Met. Ions Biol. Syst 1998;35:585–631. [PubMed: 9444770]

2. Sun H, Li H, Sadler PJ. Transferrin as a metal ion mediator. Chem. Rev 1999;99:2817–2842. [PubMed: 11749502]

3. Qian ZM, Li H, Sun H, Ho K. Targeted drug delivery via the transferrin receptor-mediated endocytosis pathway. Pharmacol. Rev 2002;54:561–87. [PubMed: 12429868]

4. Daniels TR, Delgado T, Helguera G, Penichet ML. The transferrin receptor part II: Targeted delivery of therapeutic agents into cancer cells. Clin. Immunol 2006;121:159–176. [PubMed: 16920030]

5. Mason A, He QY, Tam B, MacGillivray RA, Woodworth R. Mutagenesis of the aspartic acid ligands in human serum transferrin: lobe-lobe interaction and conformation as revealed by antibody, receptor-binding and iron-release studies. Biochem. J 1998;330:35–40. [PubMed: 9461487]

6. Giannetti AM, Halbrooks PJ, Mason AB, Vogt TM, Enns CA, Björkman PJ. The molecular mechanism for receptor-stimulated iron release from the plasma iron transport protein transferrin. Structure 2005;13:1613–1623. [PubMed: 16271884]

7. Jeffrey PD, Bewley MC, MacGillivray RT, Mason AB, Woodworth RC, Baker EN. Ligand-induced conformational change in transferrins: crystal structure of the open form of the N-terminal half-molecule of human transferrin. Biochemistry 1998;37:13978–13986. [PubMed: 9760232]

8. MacGillivray RT, Moore SA, Chen J, Anderson BF, Baker H, Luo Y, Bewley M, Smith CA, Murphy ME, Wang Y, Mason AB, Woodworth RC, Brayer GD, Baker EN. Two high-resolution crystal structures of the recombinant N-lobe of human transferrin reveal a structural change implicated in iron release. Biochemistry 1998;37:7919–28. [PubMed: 9609685]

9. Baker HM, Anderson BF, Baker EN. Dealing with iron: Common structural principles in proteins that transport iron and heme. Proc. Natl. Acad. Sci. U. S. A 2003;100:3579–3583. [PubMed: 12642662]

10. Mizutani K, Yamashita H, Kurokawa H, Mikami B, Hirose M. Alternative structural state of transferrin. The crystallographic analysis of iron-loaded but domain-opened ovotransferrin N-lobe. J. Biol. Chem 1999;274:10190–10194. [PubMed: 10187803]

11. James NG, Berger CL, Byrne SL, Smith VC, MacGillivray RTA, Mason AB. Intrinsic fluorescence reports a global conformational change in the N-lobe of human serum transferrin following iron release. Biochemistry 2007;46:10603–10611. [PubMed: 17711300]

12. Kaltashov IA, Zhang M, Eyles SJ, Abzalimov RR. Investigation of structure, dynamics and function of metalloproteins with electrospray ionization mass spectrometry. Anal. Bioanal. Chem 2006;386:472–481. [PubMed: 16932945]

13. Gumerov DR, Kaltashov IA. Dynamics of iron release from transferrin N-lobe studied by electrospray ionization mass spectrometry. Anal. Chem 2001;73:2565–2570. [PubMed: 11403301]

14. Gumerov DR, Mason AB, Kaltashov IA. Interlobe communication in human serum transferrin: metal binding and conformational dynamics investigated by electrospray ionization mass spectrometry. Biochemistry 2003;42:5421–8. [PubMed: 12731884]

15. Wales TE, Engen JR. Hydrogen exchange mass spectrometry for the analysis of protein dynamics. Mass Spectrom. Rev 2006;25:158–170. [PubMed: 16208684]

16. Kaltashov IA, Eyles SJ. Crossing the phase boundary to study protein dynamics and function: combination of amide hydrogen exchange in solution and ion fragmentation in the gas phase. J. Mass Spectrom 2002;37:557–565. [PubMed: 12112737]

17. Pan J, Han J, Borchers CH, Konermann L. Electron capture dissociation of electrosprayed protein ions for spatially resolved hydrogen exchange measurements. J. Am. Chem. Soc 2008;130:11574–11575. [PubMed: 18686958]

18. Zhang M, Kaltashov IA. Mapping of protein disulfide bonds using negative ion fragmentation with a broadband precursor selection. Anal. Chem 2006;78:4820–4829. [PubMed: 16841900]

19. Cravello L, Lascoux D, Forest E. Use of different proteases working in acidic conditions to improve sequence coverage and resolution in hydrogen/deuterium exchange of large proteins. Rapid Commun. Mass Spectrom 2003;17:2387–2393. [PubMed: 14587084]

20. He QY, Mason AB, Tam BM, MacGillivray RT, Woodworth RC. Dual role of Lys206-Lys296 interaction in human transferrin N-lobe: iron-release trigger and anion-binding site. Biochemistry 1999;38:9704–9711. [PubMed: 10423249]

21. Dautry-Varsat A, Ciechanover A, Lodish HF. pH and the recycling of transferrin during receptor-mediated endocytosis. Proc. Natl. Acad. Sci. U. S. A 1983;80:2258–2262. [PubMed: 6300903]

22. Dempsey CE. Hydrogen exchange in peptides and proteins using NMR-spectroscopy. Progr. Nucl. Magn. Res. Spectrosc 2001;39:135–170.
23. Krishna MMG, Hoang L, Lin Y, Englander SW. Hydrogen exchange methods to study protein folding. Methods 2004;34:51–64. [PubMed: 15283915]
24. Halbrooks PJ, He QY, Briggs SK, Everse SJ, Smith VC, MacGillivray RT, Mason AB. Investigation of the mechanism of iron release from the C-lobe of human serum transferrin: mutational analysis of the role of a pH sensitive triad. Biochemistry 2003;42:3701–3707. [PubMed: 12667060]
25. Egan TJ, Zak O, Aisen P. The anion requirement for iron release from transferrin is preserved in the receptor-transferrin complex. Biochemistry 1993;32:8162–8167. [PubMed: 8347616]
26. Kaltashov IA. Probing protein dynamics and function under native and mildly denaturing conditions with hydrogen exchange and mass spectrometry. Int. J. Mass Spectrom 2005;240:249–259.
27. Konermann L, Tong X, Pan Y. Protein structure and dynamics studied by mass spectrometry: H/D exchange, hydroxyl radical labeling, and related approaches. J. Mass Spectrom 2008;43:1021–1036. [PubMed: 18523973]
28. Hilser VJ, Thompson EB. Intrinsic disorder as a mechanism to optimize allosteric coupling in proteins. Proc. Natl. Acad. Sci. U.S.A 2007;104:8311–8315. [PubMed: 17494761]
29. Xie H, Vucetic S, Iakoucheva LM, Oldfield CJ, Dunker AK, Uversky VN, Obradovic Z. Functional anthology of intrinsic disorder. 1. Biological processes and functions of proteins with long disordered regions. J. Proteome Res 2007;6:1882–1898. [PubMed: 17391014]
30. Baron R, McCammon JA. (Thermo)dynamic Role of Receptor Flexibility, Entropy, and Motional Correlation in Protein-Ligand Binding. Chemphyschem 2008;9:983–988. [PubMed: 18418822]
31. Thorpe IF, Brooks CL. Molecular evolution of affinity and flexibility in the immune system. Proc. Natl. Acad. Sci. U. S. A 2007;104:8821–8826. [PubMed: 17488816]
32. Chang, C.-e. A.; McLaughlin, WA.; Baron, R.; Wang, W.; McCammon, JA. Entropic contributions and the influence of the hydrophobic environment in promiscuous protein-protein association. Proc. Natl. Acad. Sci. U. S. A 2008;105:7456–7461. [PubMed: 18495919]
33. Baker HM, He QY, Briggs SK, Mason AB, Baker EN. Structural and functional consequences of binding site mutations in transferrin: Crystal structures of the Asp63Glu and Arg124Ala mutants of the N-Lobe of human transferrin. Biochemistry 2003;42:7084–7089. [PubMed: 12795604]
34. Kaltashov IA, Eyles SJ. Studies of biomolecular conformations and conformational dynamics by mass spectrometry. Mass Spectrom. Rev 2002;21:37–71. [PubMed: 12210613]
35. Vidaud C, Gourion-Arsiquaud S, Rollin-Genetet F, Torne-Celer C, Plantevin S, Pible O, Berthomieu C, Quemeneur E. Structural consequences of binding of UO_2^{2+} to apotransferrin: can this protein account for entry of uranium into human cells? Biochemistry 2007;46:2215–2226. [PubMed: 17266333]
36. Giannetti AM, Snow PM, Zak O, Bjorkman PJ. Mechanism for multiple ligand recognition by the human transferrin receptor. PLoS Biol 2003;1:341–350.
37. Yersin A, Osada T, Ikai A. Exploring transferrin-receptor interactions at the single-molecule level. Biophys. J 2008;94:230–240. [PubMed: 17872962]
38. Wang L, Pan H, Smith DL. Hydrogen exchange-mass spectrometry: optimization of digestion conditions. Mol. Cell. Proteomics 2002;1:132–138. [PubMed: 12096131]
39. Bai Y, Milne JS, Mayne L, Englander SW. Primary structure effects on peptide group hydrogen exchange. Proteins 1993;17:75–86. [PubMed: 8234246]

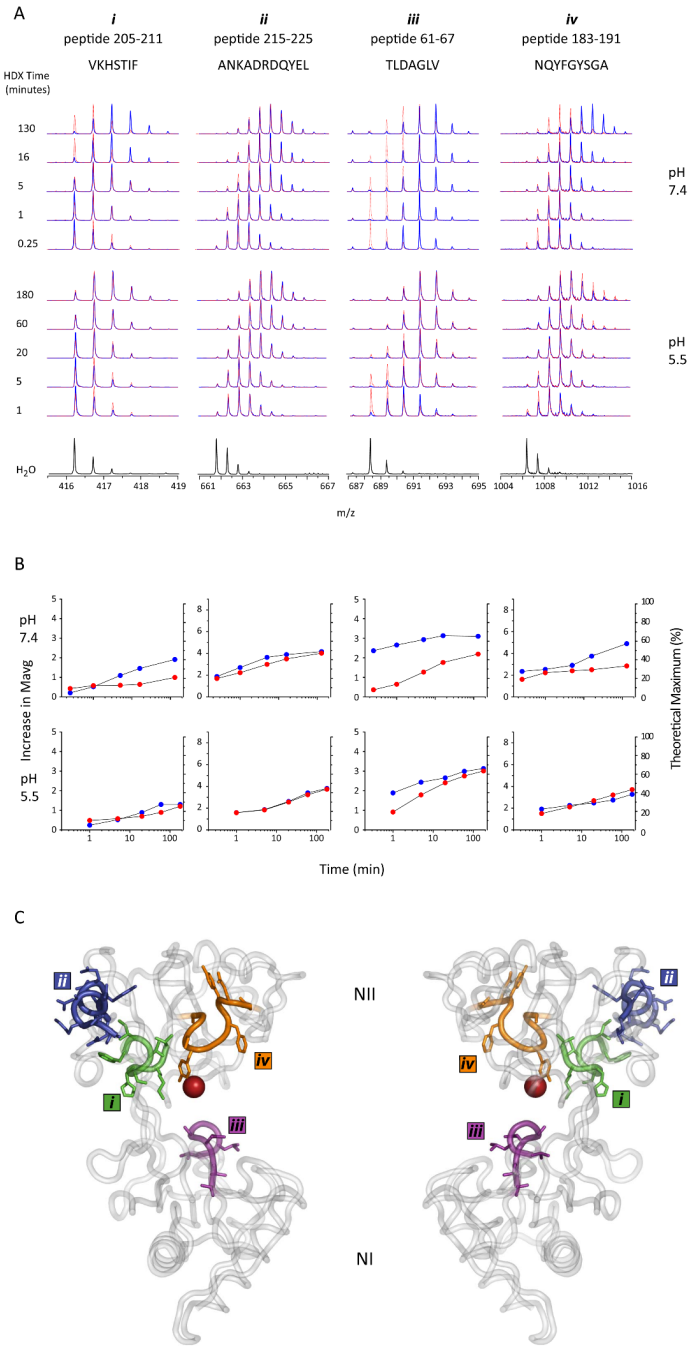

Figure 1.

Sample local HDX data. A. m/z spectra extracted from the LC-MS data for four example peptides from holo (red dotted trace) and apo (blue trace) *h*Tf/2N at the two different pH values examined. The incorporation of deuterium is observed as a shift in m/z over time compared to the non-exchanged control spectrum (labeled H_2O). B. HDX data from 1A plotted as increase in mass (y-axis on left) or % maximum exchange (y-axis on right) versus exchange time for both holo (red circles) and apo (blue circles) *h*Tf/2N. C. *h*Tf/2N crystal structure highlighting the location of the four above peptides.

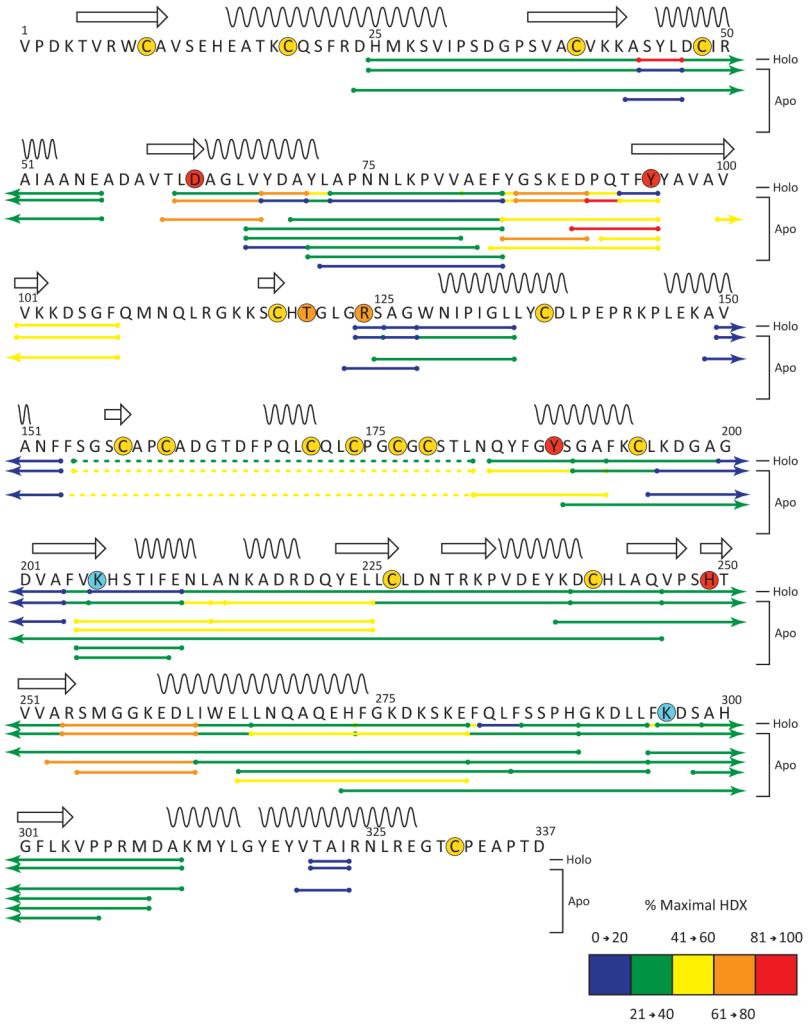

Figure 2.

Sequence Flexi-Map pH 7.4. The location of the peptides analyzed by HDX are depicted by bars below the primary structure and have been colored according to the legend based on their % maximal HDX at 5 minutes. The first two lines below the sequence represent the consolidated data for the apo and holo samples, the remaining lines below these represent all peptides analyzed per sample and are colored according to results obtained for the apo sample. Secondary structural elements helices (wavy lines) and sheets (arrows) are indicated above the sequence and various residues of interest have been highlighted by a colored circle to depict: disulfide linkage (yellow), iron binding (red), anion binding (orange), and the dilysine trigger (cyan). Peptides containing disulfides detected in their non-reduced form are indicated by a dotted line.

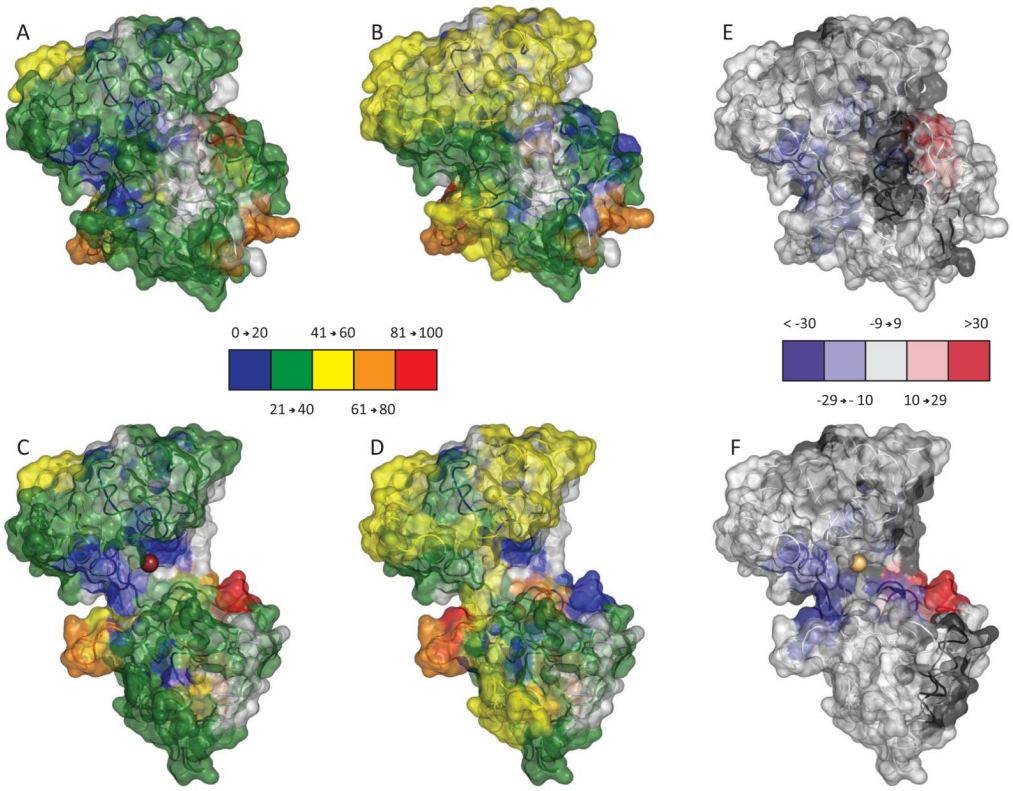

Figure 3.

Structural Flexi-Map pH 7.4. Data from the 5 minute time point were mapped to both the closed (top) and open (bottom) crystal structures and colored according the legends. To readily compare HDX between the Holo sample (A and C) and the Apo sample (B and D), the difference in % exchange (Holo – Apo) is also shown (E and F).

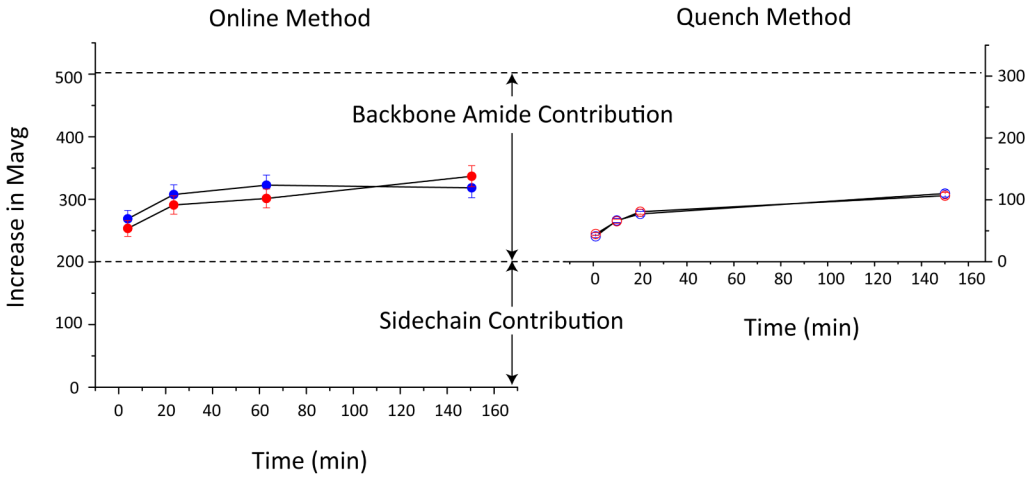

Figure 4.

Global HDX at pH 5.5. Extent of exchange data were collected to compare apo- (blue) and holo- (red) *h*Tf/2N using either a direct online method (left) or after first quenching the exchange reaction (right).

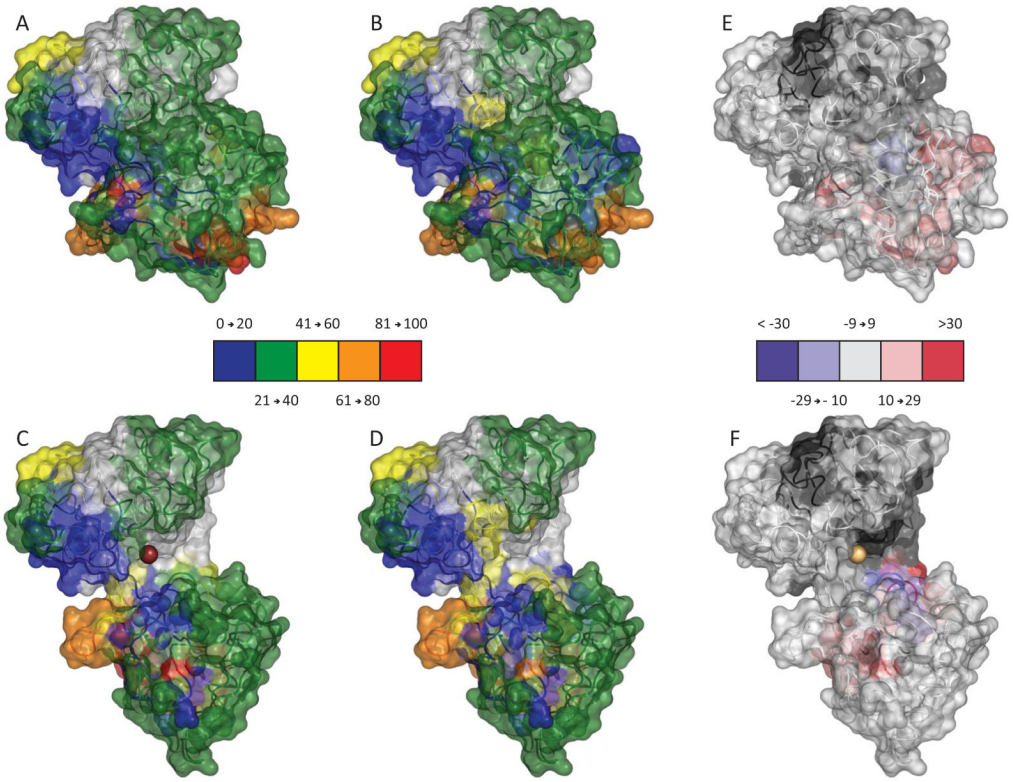

Figure 5.
Structural Flexi-Map pH 5.5. Data from the 5 minute time point were mapped to both the closed (top) and open (bottom) crystal structures and colored according the legends. To readily compare HDX between the Holo sample (A and C) and the Apo sample (B and D), the difference in % exchange (Holo – Apo) is also shown (E and F).

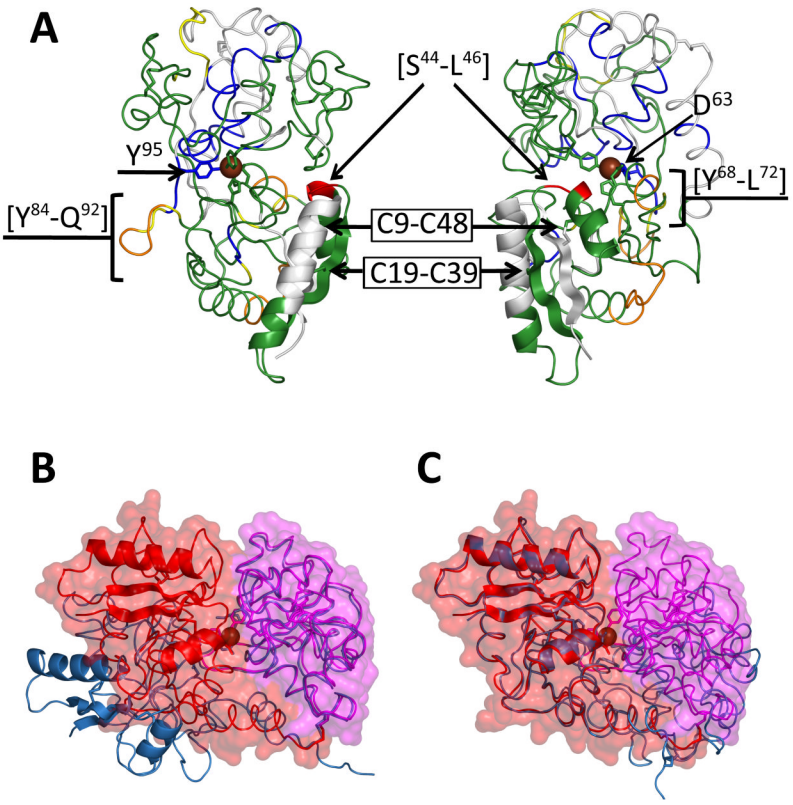

Figure 6.

Regions of increased flexibility or stability. Data from the 5 min time point of holo *h*Tf/2N were used to color the closed form of the structure shown from two different angles (A). Overlay of the open and closed forms of *h*Tf/2N to highlight the structural similarity observed in domain NI when superimposed (B and C).